

# Characterization of Post-infarct Scars in a Porcine Model – A Combined Experimental and Theoretical Study

Mihaela Pop<sup>1</sup>, Maxime Sermesant<sup>2,3</sup>, Tommaso Mansi<sup>2</sup>, Eugene Crystal<sup>1</sup>,  
Jay Detsky<sup>1</sup>, Yuesong Yang<sup>1</sup>, Paul Fefer<sup>1</sup>, Elliot R. McVeigh<sup>4</sup>, Alexander Dick<sup>1</sup>,  
Nicholas Ayache<sup>2</sup>, and Graham A. Wright<sup>1</sup>

<sup>1</sup> Sunnybrook Health Sciences Centre, University of Toronto, Canada  
mihaela.pop@utoronto.ca, gawright@sri.utoronto.ca

<sup>2</sup> ASCLEPIOS project, INRIA Sophia Antipolis, France

<sup>3</sup> Division of Imaging Science, King's College, London, UK

<sup>4</sup> Dept of Biomedical Engineering, Johns Hopkins University, Maryland, USA

**Abstract.** Arrhythmias are often associated with healing infarcts and could arise from the border zone of the scars. The main purpose of this work was to characterize the infarct scars using in vivo electro-anatomic CARTO maps (recorded in sinus rhythm) and high-resolution ex-vivo MR images in a porcine model of chronic infarct. The MR images were segmented into scar, peri-infarct and healthy ventricular tissue, and, in select slices, the results of segmentation were validated against histology. Further, the segmented volumes and associated fiber directions (derived from diffusion-weighted (DW) MRI as well as from synthetic models), were used as input to a simple two-variable mathematical model that calculates the propagation of depolarization waves and isochronal maps; and these isochronal maps were compared to the measured ones. We further correlated the size of the scar measured during the electrophysiology (EP) study with scar dimensions obtained from MRI using ex-vivo DW-MRI methods. Finally, we present preliminary results from a qualitative comparison between the scar delineation from ex vivo and in vivo MR images.

**Keywords:** Cardiac MR imaging, electrophysiology, computer modeling.

## 1 Introduction

Post-infarction arrhythmias like ventricular tachycardia (VT) and fibrillation could be lethal if not diagnosed and treated properly [1]. In the majority of cases, the peri-infarct (also known as border zone) contains viable bundles (interdigitated within dense collagenous scars) forming channels that facilitate conduction of the electrical excitation wave within and around the scars [2]. This circuit facilitates an abnormal re-excitation of the tissue, resulting in dangerous, high heart rates. The danger for arrhythmias arises from the fact that the peri-infarct zones are viable but of reduced electrical coupling between the cells; this fact is accompanied by changes in myocardium anisotropy due to the deposition of collagen between surviving bundles (consequently, the electrical propagation is altered in this area in the settings of the chronic infarct, >4 weeks).

The arrhythmogenic substrate is usually identified during an electrophysiology (EP) study; however, the current clinical technology (e.g. CARTO used in the EP laboratory is limited to surfacic endocardial and/or epicardial maps obtained using long, invasive procedures performed under fluoroscopy [3]. Moreover, many patients are hemodynamically unstable and therefore the arrhythmogenic substrate is mapped only during sinus rhythm (without inducing VT); thus the substrate is often missed and hence cannot be treated via RF ablation [4].

There is a strong clinical motivation to supplement the electrophysiology measurements with accurate 3D anatomical information, as well as to characterize the infarct heterogeneity. Efforts have been made to characterize the post-infarct scars using imaging techniques like MRI and PET. For instance, using diffusion-weighted MRI methods, it was demonstrated in ex-vivo formalin-fixed porcine hearts that the regions of increased apparent diffusion coefficient (ADC) correlated very well with dense scars [5]. Similar findings were seen in patients with prior myocardial infarct. However, motion artifacts affect in-vivo imaging; thus ADC maps and fiber directions cannot be obtained accurately and with high spatial resolution [6]. Another recent study has demonstrated the excellent capabilities of delayed-enhanced MRI to delineate 3D anatomical scars, with fine differentiation between the core infarct and the peri-infarct (i.e., border zone) in ex-vivo porcine hearts. Tissue heterogeneity correlated well with the arrhythmogenic substrate identified from activation maps recorded in vivo in this model [7]. Progress has also been made on the clinical side, and it was shown in small cohorts of patients [8] that the peri-infarct zone size is a powerful predictor of infarction mortality. In this study, the areas of delayed enhancement were subdivided into "core" and "peri-infarct" zones on the basis of differences in signal intensity (core zone = signal  $\geq 3$  SD above that in remote non-infarcted myocardium, and peri-infarct zone = signal 2 to 3 SD above that in remote myocardium). Moreover, other clinical groups showed that the 3D anatomical information reconstructed from MRI [9] and PET [10] give a better delineation of the infarct/peri-infarct areas than the surfacic CARTO maps. However, these studies lack the histological validation for image measures of infarct heterogeneity [7, 8, 11]; furthermore, the thresholds associating EP measurements with infarct scar need to be better defined [3, 9].

Computer modelling has been extensively used in electrophysiology to predict the electrical activity in healthy hearts as well as in pathologic cases [12]. For instance, a simple mathematical model of cardiac electrical propagation (i.e., the two-variable model developed by Aliev & Panfilov [13]) which solves for the transmembrane potential and calculates the propagation of a depolarization wave, has been used to perform electro-mechanical simulations on a 3D healthy heart model [14] and with reentrant substrates [15]. It was also used to build maps of local apparent electrical conductivity by integrating information from measurements obtained via a multi-electrode sock in an in-vivo dog heart model [16]. Most of the cardiac models account for tissue anisotropy, and the fiber directions are often obtained via DW-MRI. Synthetic fibers derived from population data may also be useful when the DW-MRI data is not available but their accuracy remains to be tested.

Our broad aim is to characterize the post-infarction scars using electro-anatomic CARTO maps augmented with 3D information from MR imaging, and to complement this with insights from theoretical modelling. In the current work, we focus on: i)

building such a model from MRI; ii) comparing the scar dimensions in the model and anatomic CARTO maps; and iii) qualitatively comparing the theoretical predictions (e.g. isochronal maps) with those measured during the EP study. Figure 1 illustrates the workflow.

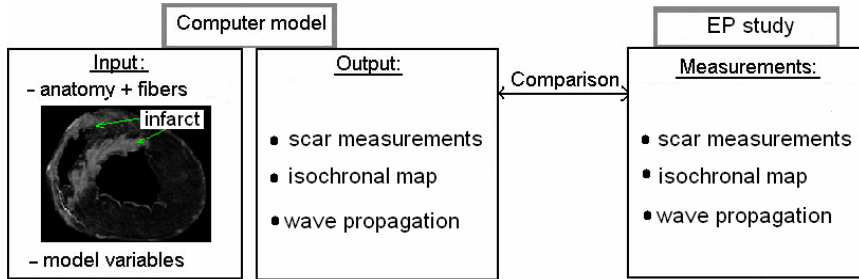


**Fig. 1.** Diagram of the comparison between the computer model and experiments

## 2 Methodology

We describe below the experimental steps following the order in which they were performed. We first completed the *in vivo* EP studies. We then explanted the hearts and used DW-MRI to characterize the infarct heterogeneity, as well as to derive the myocardial fiber directions. The segmented volumes were further used to construct the computer model. Next, the simulations were performed with parameters assigned by zones defined from the segmentation procedure. To validate the segmentation step, whole-mount histology was performed in select heart slices cut in short-axis.

### 2.1 EP Study

The animals (6 swine) had myocardial infarcts (MI) generated by a 90min coronary artery occlusion followed by reperfusion (in accordance to the animal research protocol guidelines approved by Sunnybrook Health Sciences Centre). Three animals had the left anterior descending (LAD) artery occluded, while the left circumflex (LCX) artery was occluded in the other three. The *in vivo* EP studies of the healing MI were performed at 4-5 weeks post-occlusion.

### 2.2 Magnetic Resonance Imaging and Segmentation

At the completion of the EP study, the hearts were explanted, gently preserved in formalin, and imaged using a 1.5Tesla Signa GE MR scanner for anatomy, scar characterization and myocardial fiber directions, using the MR pulse sequence described in [17]. In this work, we used the following MR parameters: TE=32ms, TR=700ms, NEX=1,  $b$ -value  $\sim 600$ , 7 directions for diffusion gradients, FOV/matrix =10cm, 256x256 acquisition matrix, and 2mm slice thickness. The heart anatomy was extracted from the un-weighted images (i.e.,  $b=0$ ) and used to generate the volumetric mesh for the mathematical model. Next, the apparent diffusion coefficient (ADC) maps were calculated using MedINRIA software and further analyzed by segmenting the heart to study the tissue heterogeneity. For segmentation, we have adapted the

expectation-maximization (EM) algorithm described in [18], which is initialized using a 3-class k-means clustering. After identification and removal of the outliers, the final segmented image contains three zones: healthy tissue, peri-infarct and infarct (dense scar). The synthetic fibers were computer generated based on well known variations of myocardial fibers from epicardium to endocardium [6, 17, 19]. The segmentation analysis, as well as the calculations of fiber directions were performed with Matlab (Mathworks, CA).

### 2.3 Histology

Representative slices cut in short-axis view were prepared for whole-mount histology and stained with Mason's Trichrome to enable the visualization of collagenous fibers. The samples (cut at  $5\mu\text{m}$ ) were scanned at 2-10 $\mu\text{m}$  resolution.

### 2.4 Computer Model

We use the cardiac mathematical model developed by Aliev and Panfilov. In the system of equations given in (1-2) we solve for the action potential ( $V$ ) and recovery variable contribution ( $r$ ). The term  $-kV(V-a)(V-I)$  controls the fast processes (initiation and upstroke of action potential) via the threshold parameter  $a$ , while  $r$ , determines the dynamics of the repolarization phase.

$$\frac{\partial V}{\partial t} = \nabla \cdot (D\nabla V) - kV(V-a)(V-I) - rV \quad (1)$$

$$\frac{\partial r}{\partial t} = -\left(\varepsilon + \frac{\mu_1 r}{\mu_2 + V}\right)(ku(u-a-1) + r). \quad (2)$$

Most of the parameters (i.e.  $\varepsilon=0.01$ ,  $a=0.1$ ,  $k=8$ , and  $\mu_2=0.3$ ) were set to reproduce the shape, duration and restitution of action potentials (AP) as in [15]. This model accounts for the heart anisotropy via the diffusion tensor,  $D$ , which depends on a tissue's conductivity, set to 1 for a normal/healthy conduction and 0 for infarct areas. The value in the anisotropy ratio (a parameter in the diffusion tensor  $D$ ) is set to 0.25 for a wave propagating twice as fast along the fiber as in the transverse direction.

The heart surface mesh was created from the anatomy images using classical segmentation algorithms (thresholding, mathematical morphology, marching cubes). Then, the volumetric tetrahedral mesh was generated with the GHS3D package (INRIA, France). We solved for the transmembrane potential using the Finite Element Method, with an explicit Euler time integration scheme. The code was written in C++ and uses OpenGL libraries to display the results.

## 3 Results

### 3.1 Model Building from DW-MRI

Figure 2 shows fiber directions obtained from DW-MRI, for a heart with LAD-occlusion (a) and LCX occlusion (c), respectively. The remarkable changes in fiber directions in the settings of the chronic infarct were due to ventricular re-modelling and can be observed by direct comparison with synthetic fibers (the latter being

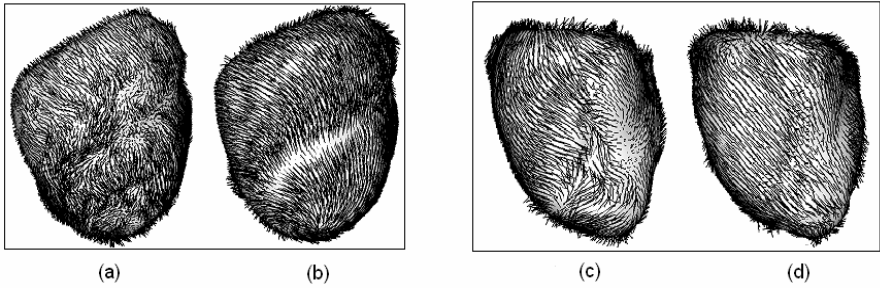


**Fig. 2.** Fibers reconstructed from DW-MRI (a) and (c), and synthetic fibers (b) and (d)

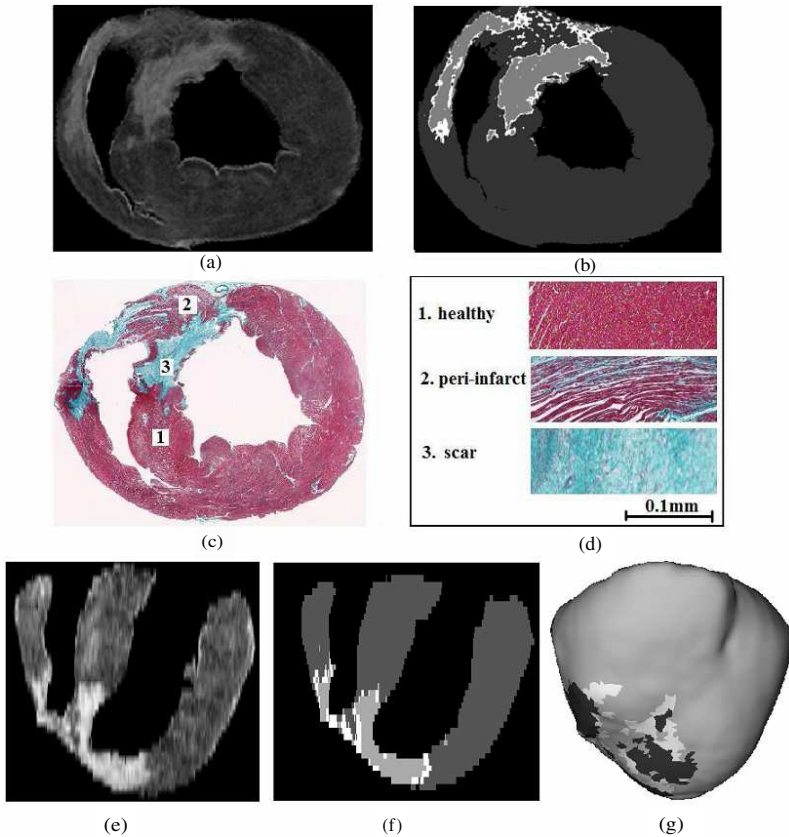


**Fig. 3.** A representative slice from the LAD-MI showing: short-axis ADC map from DW-MRI (a), its corresponding segmentation using the EM algorithm (b) as well as the corresponding Mason's Trichrome histology (c) with example areas from the healthy myocardium, peri-infarct, and dense/collagenous scar (d). A long axis slice of ADC map (e) and its segmentation (f) as well as the 3D volumetric reconstructed heart (g).

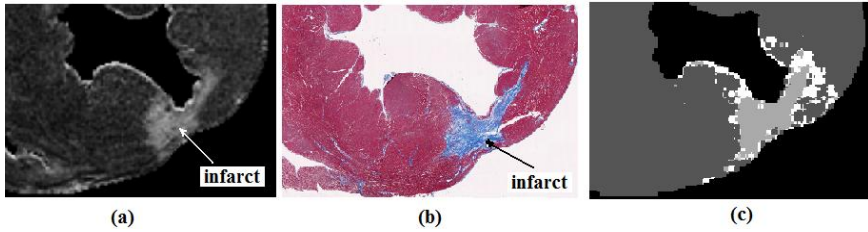


**Fig. 4.** A representative slice from the LCX-MI showing: ADC map from DW-MRI (a), corresponding histology (b) and the segmented slice (using the EM algorithm) (c)

generated from healthy hearts) displayed in Fig 2 b, and d, respectively. Note that for the cardiac computer model, the fiber directions were specified at the baricenter of each tetrahedral element of the computational mesh.

Figures 3 and 4 give examples of the model construction from the segmented ADC obtained in two hearts. The bright areas in Fig 3a and 4a, correspond to an expected increase in ADC values in the scar and peri-infarct. Histological analysis revealed on microscopic observation that infarct areas remodeled over time. Dense scars (stained in green/blue color in Figs 3c-d and 4b) have necrotic myocytes and large zones with myocytes replaced by dense fibrosis (in green-blue) accompanied by a complete loss of anisotropy. The peri-infarct areas have mixed islands of viable and non-viable myocytes, as well as fiber directions slightly changed due to droplets of collagen deposits between surviving cardiac myocytes (viable myocytes in red) (Fig 3d). The infarct heterogeneity was very well identified by the EM algorithm (see white areas in Figs 3b,f and 4c corresponding to peri-infarct, and light-grey areas corresponding to dense scar).

In the model, the conductivity term controls the degree of cellular uncoupling; thus, the infarct zone is modeled as a zone of zero electrical conductivity. As a result, the scar does not propagate the excitation wave regardless of the fiber directions in the scar. In the peri-infarct zone, the conductivity is reduced compared to that of normal myocardium and the wave will propagate through the peri-infarct, but at a slower rate so that direction of the wave front is influenced by the fiber orientation.

### 3.2 Comparison between Experiments and Theoretical Model

Voltage maps were constructed from CARTO epicardial recordings, using the usual cut-off threshold at  $<0.5\text{mV}$  for infarct (red),  $0.5\text{-}1.5\text{mV}$  border zone (peri-infarct, green-blue) and  $>1.5\text{mV}$  healthy tissue (purple), with an example provided in Fig 5a for LAD-MI. The scar (measured on the epicardium) was  $13.1\text{cm}^2$  on the CARTO map vs.  $11.5\text{cm}^2$  in MRI.

Moreover, the activation times can be represented by isochrones (lines connecting pixels of equal activation time). Isochronal maps can be produced over one heart beat; an example is presented in Figure 4.b-d. The isochrones calculated from the bipolar recordings (b) agreed reasonably well with those from simulated activation times (displayed on the mesh for the fibers obtained from DW-MRI (c) and the synthetic fibers (d)). For the simulations in this study, we used a computational time step of

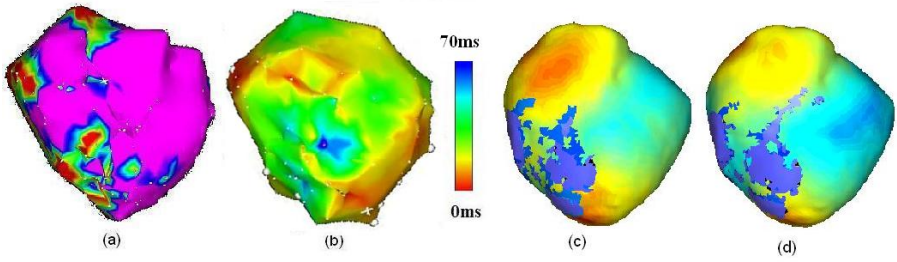


**Fig. 5.** Voltage map (CARTO) of the LAD-MI(a); isochronal maps generated from bipolar recordings (b) and simulated isochrones on the mesh with fibers from DW-MRI (c) and synthetically generated (d), where then red areas correspond to early activation times

$1 \times 10^{-4}$ s. The simulation time for 0.8s on a mesh of approximately 230,000 elements (~1.2mm element size) is about 1h on an Intel® Core™2 duo CPU, T5550 @1.83GHz, with 4Gb of RAM.

Results are also illustrated for an LCX-MI heart in Fig. 6, where the scar (in red) and border zone (in green-blue) is measured to be  $<1\text{cm}^2$  using electro-anatomic CARTO voltage maps on the endocardium (a) and  $2.3\text{cm}^2$  on the epicardium (b). The epicardial scar ( $2.2\text{cm}^2$ ) from segmentation of MR images is shown on the reconstructed 3D model (c); although not shown, the endocardial scar was measured to be  $2.4\text{cm}^2$  from MR images.

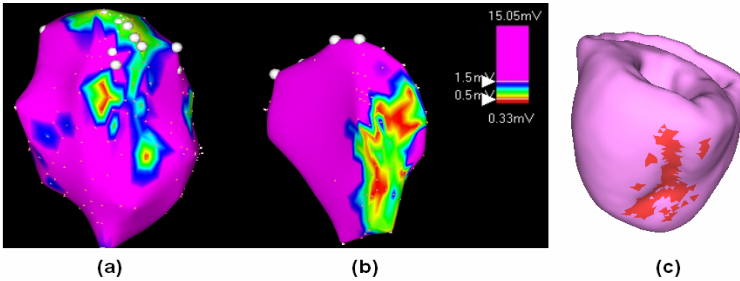


**Fig. 6.** Scar (red color) delineation in voltage maps (CARTO) of an LCX-MI: endocardial (a) and epicardial (b) maps, and on the 3D heart model (c)

## 4 Discussion and Future Work

In this work we report results for MRI characterization of post-infarct scars in a porcine model and associated electrophysiology. Experimental results obtained from ex vivo measurements demonstrated that infarct heterogeneity is well characterized by DW-MRI methods. The infarct areas can be segmented using the E-M algorithm, and good qualitative correlation was as proved by the histological analysis. Here, the logical next step will be to quantify the model-predicted scar against the Mason’s Trichrome stain that we used. In particular, this stain will permit the quantification of collagen/fibrosis (which is related to the electrical uncoupling of the cells). In the

future, we will perform a comparison between the areas of these three segmented zones against corresponding identified areas in the histological images. A few methods based on color thresholding are available for microscopic image analysis and will be explored in the future. Further, the segmented images served to build a 3D volumetric model of the heart that was used to calculate the scar dimensions and compare them with measured size from CARTO voltage maps; this could help in the calibration of the voltage thresholds for infarct (which are still ambiguous in the EP study).

The model developed by Aliev&Panfilov is not a biophysical model, but rather rapidly computes, at a macroscopic scale, the propagation of depolarization wave, from which the isochronal maps can be calculated and compared with isochrones from electrical measurements. Our initial results showed good correspondence between the model and experimental measures. However, results were limited by the fact that we did not register the CARTO anatomical images with the MR images; thus localization of errors was not performed. In CARTO images we will quantify the scar and peri-infarct using either the voltage maps or isochronal maps, or a combination of both, exactly as per the method provided in [9]. An image-based model was recently successfully constructed to characterize the atrium excitation [20]; for accurate comparisons, such estimations should be included. Obviously, the *in vivo* MR images will help identifying the scars areas; thus the CARTO maps will be recorded with a higher density around the border zone of the infarct. Then, a registration will be performed: a) for the endocardial maps we will use anatomical markers (i.e. valves, apex) to register the model-based surfaces (RV, LV) to the CARTO endocardial surface (as per the method provided in [9]), and b) the epicardial surface will be registered to the model by a method that we have previously developed and used to register the anatomic model to epicardial surfaces derived via optical images [21]. The epicardial map is recorded during open chest procedure (in our current CARTO experiment), and that makes it easy to glue opaque markers (which are visible in the MRI) onto the exposed surface; the markers location can then be used for a rigid registration between the CARTO surface and the epicardial surface of the heart model (as in [21]).

Our efforts are also being extended to building a 3D model from *in-vivo* MRI data. For instance, Fig.7 presents a preliminary result comparing the left ventricle segmentations of an *in-vivo* MR image using multi-contrast delayed enhancement

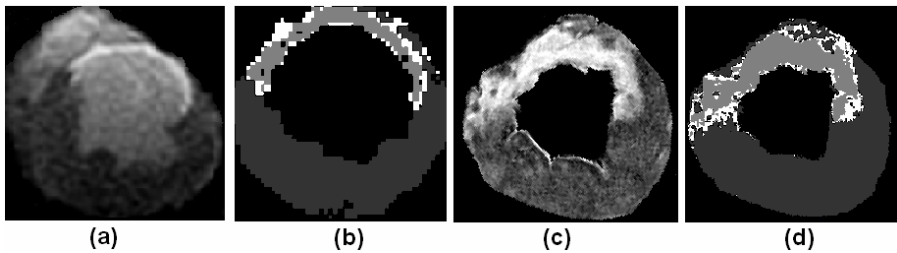


**Fig. 7.** Comparison between segmentation of *in vivo* MCDE and *ex vivo* DW-MR images

(MCDE) method developed in our laboratory [22] and a corresponding ex vivo DW-MR image. While good agreement was found, next steps include obtaining higher resolution in vivo images, as well as characterizing and segmenting the scars involving the right ventricle. "Heterogeneous" areas were identified in DE-MRI by Ashikaga et al [7] in ex vivo images acquired with a resolution of 0.4x0.4x0.4mm as well as by Yan [8] in humans (using a 8-mm slice thickness). In our studies we focus on regions which are more than 1 pixel wide, reducing the likelihood that partial voluming between two distinct tissue regions dominates we focus on regions which are more than 1 pixel wide, reducing the likelihood that partial voluming between two distinct tissue regions dominates. To demonstrate further that partial voluming effects do not dominate in the highlighted regions, we plan to perform experiments with a smaller slice thickness in the future (currently we are using a 2-mm slice thickness for the ex vivo DTI method and 5mm for the in vivo MCDE).

To conclude, the validation and calibration of fast computer models is ongoing; this is an important step prior to their integration into clinical applications (i.e. diagnosis and therapy planning); scar characterization obtained from ex vivo imaging data is useful in facilitating this validation / calibration phase. The goal of these models is to be used in combination with less invasive imaging and EP diagnostic procedures, to improve the outcome of the therapy and its success rate [23]. Minimal amount of imaging time and pre-operative processing is desired; our model is highly adaptive and ultimately will be fitted to patient data. One limitation will be the lack of the fiber directions data, but models with synthetic fibers can be used instead. We also envision that MRI combined with limited information (e.g. 12-lead ECG) as in [24], together with the theoretical characterization of action potential propagation, will be enough to diagnose many of the scar-related diseases.

## References

1. Kebler, A., Rudy, Y.: Basic mechanisms of cardiac impulse propagation and associated arrhythmias. *Physiological Review* 84, 431–488 (2004)
2. Ursell, P.C., Gardner, P.I., et al.: Structural and electrophysiological changes in the epicardial border zone of canine myocardial infarcts during healing. *Circ. Research* 56, 436–451 (1985)
3. Arenal, A., del Castillo, S., Gonzalez-Torrecilla, E., et al.: Tachycardia-related channel in the scar tissue in patients with sustained monomorphic VT. Influence of the voltage scar definition. *Circulation* 110, 2568–2574 (2004)
4. Ciaccio, E.J., Chow, A.W., Kaba, R.A., et al.: Detection of the diastolic pathway, circuit morphology, and inducibility of human postinfarction VT from mapping in sinus rhythm. *Heart Rhythm* 5(7), 981–991 (2008)
5. Wu, E.X., Wu, Y., et al.: MR diffusion tensor imaging study of postinfarct myocardium structural remodeling in a porcine model. *Magnetic Resonance Medicine* 58(4), 687–695 (2007)
6. Wu, M.T., Tseng, W.Y., Su, M.Y., et al.: Diffusion tensor magnetic resonance imaging mapping the fiber architecture remodeling in human myocardium after infarction: correlation with viability and wall motion. *Circulation* 114, 1036–1045 (2006)
7. Ashikaga, H., Sasano, T., Dong, J., et al.: MR based anatomical analysis of scar-related VT. *Circulation Research*, 1–9 (2007)

8. Yan, A.T., Shayne, A.J., Brown, K.A., et al.: Characterization of the Peri-Infarct Zone by Contrast-Enhanced Cardiac MRI is a powerful predictor of Post-Myocardial infarction mortality. *Circulation* 114, 32–39 (2006)
9. Codreanu, A., Odille, F., Aliot, E., et al.: Electroanatomic characterization of post-infarct scars. Comparison with 3D myocardial scar reconstruction based on MRI. *Journal of the American College of Cardiology* 52(10), 839–842 (2008)
10. Dickfield, T., Lei, P., Dilsizian, V., et al.: Integration of 3D scar maps for VT ablation with PET-Computed tomography. *Cardiovascular Imaging* 1(1), 73–82 (2008)
11. Nazarian, S., Bluemke, D.A., Lardo, A.C., et al.: Magnetic resonance assessment of the substrate for inducible VT in nonischemic cardiomyopathy. *Circulation* 112(18), 2821–2825 (2005)
12. Clayton, R.H., Panfilov, A.V.: A guide to modelling cardiac electrical activity in anatomically detailed ventricles. *Progress in Biophysics & Molecular Biology* (review) (2007)
13. Aliev, R., Panfilov, A.V.: A simple two variables model of cardiac excitation. *Chaos, Soliton and Fractals* 7(3), 293–301 (1996)
14. Nash, M.P., Panfilov, A.V.: Electromechanical model of the excitable tissue to study reentrant cardiac arrhythmias. *Progress in Biophysics and Molecular Biology* 85, 501–510 (2004)
15. Sermesant, M., Delingette, H., Ayache, N.: An Electromechanical Model of the Heart for Image Analysis and Simulation. *IEEE Trans. on Med. Imag.* 25(5), 612–625 (2006)
16. Moreau-Villeger, V., Delingette, H., Sermesant, M., Ashikaga, H., McVeigh, E.R., Ayache, N.: Building maps of local apparent conductivity of the epicardium with a 2-D electrophysiological model of the heart. *IEEE Transactions on Biomedical Engineering* 53(8), 1457–1466 (2006)
17. Helm, P., Tseng, H.J., Younes, L., McVeigh, E.R., Winslow, R.L.: Ex vivo 3D diffusion tensor imaging and quantification of cardiac laminar structure. *Magn. Res. Med.* 54, 850–859 (2005)
18. Van Leemput, Maes, K., Vandermeulen, F., et al.: Automated segmentation of multiple sclerosis lesions by model outlier detection. *IEEE Trans. on Medical Imaging* 20(8), 677–688 (2001)
19. Arts, T., Costa, K.D., Covell, J.W., et al.: Relating myocardial laminar architecture to shear strain and muscle fiber orientation. *Cardiovascular Research Institute* 280(5), 2222–2229 (2001)
20. Tilg, B., Fischer, G., Modre, R., Hanser, F., et al.: Model-based imaging of cardiac electrical excitation in humans. *IEEE Transactions on Medical Imaging* 21(9), 1031–1039 (2002)
21. Pop, M., Sermesant, M., Lepiller, D., et al.: Fusion of optical imaging and MRI for the evaluation and adjustment of macroscopic models of cardiac electrophysiology: a feasibility study. *Medical Image Analysis* (2008) (July 25, E-Pub. ahead of print)
22. Jay, D.S., Stainsby, J.A., Vijayaraghavan, R., Graham, J.J., Dick, A.J., Wright, G.A.: Inversion-recovery-prepared SSFP for cardiac-phase-resolved delayed-enhancement MRI. *Magn. Res. Med.* 58(2), 365–372 (2007)
23. Sermesant, M., Peyrat, J.M., Chinchapatnam, P., Billet, F., Mansi, T., Rhode, K., et al.: Toward patient-specific myocardial models of the heart. *Heart Fail Clin.* 4(3), 289–301 (2008)
24. Strauss, D.G., Wu, K.C.: Imaging myocardial scar and arrhythmic risk prediction – a role for the electrocardiogram? *J. Electrocardiol.* 42(2), 138.e1–8 (2009)